Prediction of air flow noise in ducts due to the presence of fixed obstacles

Nicolas Papaxanthos, Emmanuel Perrey-Debain, Boureima Ouedraogo, Solène Moreau, Jean-Michel Ville, Felix Foucart
Sorbonne Universités, Université de Technologie de Compiègne, Laboratoire Roberval UMR CNRS 7337, CS 60 319, 60 203 Compiègne cedex, France

Saâd Bennouna
Valeo Thermal Systems, 8 rue Louis Lormand, 78320 La Verrière, France.

Summary
This work deals with noise produced by interaction of a low Mach number flow with fixed obstacles inserted in a rectangular duct. Computation of flow generated noise is accomplished following a hybrid approach. First, results of a CFD simulation using unsteady incompressible LES are compared with measurements using laser PIV system. The procedure allows to compare mean flow velocities as well as turbulence kinetic energy. In a second step, the total pressure which includes compressibility effects, is calculated via the Lighthill-Curle analogy. Predicted Sound Pressure Levels are compared with measurements in the case of a diaphragm. Modal radiated sound powers are also illustrated.

PACS no. 43.28.Py

1. Introduction

The prediction of flow noise in ducts is necessary for noise control in industrial ducts, such as HVAC or pipelines. In many instances, the presence of a singularity in a duct such as a sharp bend, a constriction (orifice, diaphragm) or an obstacle (flap, splitter) will result in unsteady aerodynamics generating propagating sound waves along the duct. The present work deals more specifically with the noise produced by a thin-walled diaphragm inserted in a rectangular duct containing a low Mach number flow. This configuration has been studied by many authors since the pioneering work of Nelson *et al.* [1] who derived scaling laws for the acoustic power. In this regard, we can cite recent work of Kårekull *et al.* [2] and Mak *et al.* [3] who proposed improved formulations based on fast Computational Fluid Dynamics (CFD) models such as Reynold-average Navier-Stokes (RANS) simulations. Numerical predictions can also be obtained at a heavier price (in terms of CPU time and computing facilities) by solving the full Navier-Stokes equations for compressible flows [4]. Because of the relatively low Mach and large Reynolds numbers that characterize the flow, most existing commercial softwares propose an hybrid method to calculate the generated sound. It consists in an incompressible Large Eddy Simulation (LES) of the turbulent flow, during which aerodynamic quantities are recorded. In a second step, an aeroacoustic analogy is solved, this can be either the classical Lighthill's equation [6] using a variational approach [5] or the Curle's equation [7] using the Boundary Element Method (BEM) [8]. The method used in this work falls into the second category. It shares some similarities with [9] except it has been specifically designed for predicting the multi-mode propagation and generation of sound waves in an infinite duct. The general methodology (CFD calculations and the acoustic analogy) as well as the measurement procedures including the use of the Particle Image Velocimetry (PIV) are now explained.

2. Flow simulation

The CFD commercial software STAR-CCM+ is used for CAO modeling and mesh generation. The geometry of interest consists of a duct with a rectangular cross-section 20 cm x 10 cm. The diaphragm illustrated in Figures 1 and 2 is a 10 cm $\times$ 5 cm constriction centered in the duct. Its thickness is 8 mm. The inlet is located at 0.3 m and the outlet at 1.6 m from the singularity. CFD calculations using successively about 1, 3, 5, 7 and 10 millions cells have been performed. It was found that acoustic results have converged when using 5 millions cells. The corresponding

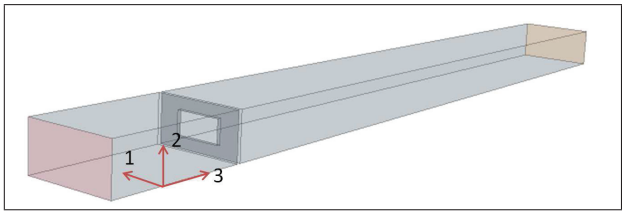

Figure 1. CAO: duct and diaphragm.

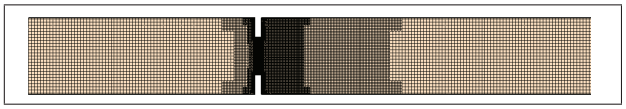

Figure 2. Mesh in the midplane.

Table I. Mesh parameters used with STAR-CCM+.

Template	Hexahedral
Base size	5 mm
Surface size	[1 : 4.5] mm
Surface size on diaphragm	0.5 mm
Number of boundary layers	5
Boundary layer thickness	0.5 mm
Thickness of near wall prism layer	0.002 mm
Total number of cells	5.08 M
Minimum cell quality [0 : 1]	0.23

Table II. RANS parameters.

Turbulence model	$k-\epsilon$
Time calculation	7 min (1500 iterations)

Table III. LES parameters.

Turbulence model	LES Wale subgrid scale
Time step	10^{-5} s
Simulated physical time	0.5 s
Time calculation	29h48min

main mesh parameters are reported in Table I.

A RANS simulation is first performed as an initial condition for an incompressible LES. The main parameters of the simulations can be found in Tables II and III. All calculations are carried out on 160 CPU cores in parallel and the whole process (CFD and acoustic analysis) does not exceed 2 days. Inlet conditions are prescribed using velocity components and turbulence kinetic energy which are provided by the PIV results. In the configuration tested here, the average velocity over the inlet cross-section is equal to 6.5 m/s. At the outlet, standard static pressure conditions are prescribed. For the acoustic calculations (as shown later), pressure at boundaries is recorded with a time step of 10^{-4} s which is sufficiently small to ensure that the frequency range of interest (up to 3500 Hz) is covered.

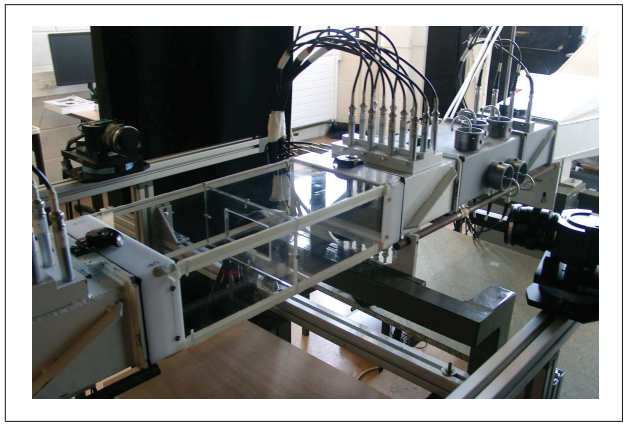

Figure 3. Test bench with PIV instruments.

3. Flow field analysis

Aerodynamic quantities (which include mean flow velocity field and wall pressures) are measured on an acoustic test bench developed during the CESAM and CEVAS projects [10, 11]. For the sake of illustration Figure 3 shows the PIV instruments and two sets of microphones located upstream and downstream with respect to the diaphragm. PIV system is a non-intrusive optical method for flow velocity measurements [12] around the component. It requires a pulsed laser and 2 CCD cameras for 3D measurements. Our laser is a double pulsed Nd-YAG type of 532 nm wavelength with a 15 Hz operating frequency. This relatively slow frequency signifies that only averaged quantities can be extracted.

Applying Reynolds decomposition to transverse and streamwise velocities, mean velocity vectors are obtained as

$$\mathbf{V} = \langle u_2 \rangle \mathbf{e_2} + \langle u_3 \rangle \mathbf{e_3} \quad \text{and} \quad u_i = \langle u_i \rangle + u'_i . \quad (1)$$

Figures 4 shows a comparison of the velocity vectors near the constriction over the (x_2, x_3) plane located near the middle of the duct at $x_1 = 0.092$ m. The LES simulation shows very good agreement with PIV measurements (especially the flow past the vena contracta) showing two identifiable recirculation zones. It can be noted that the RANS result shows substantial departures from the measured data.

The mean turbulence kinetic energy

$$k = \frac{\langle {u'_1}^2 \rangle + \langle {u'_2}^2 \rangle + \langle {u'_3}^2 \rangle}{2} \quad (2)$$

gives an indication of the location of turbulence structures and their intensity. This quantity plays a significant role in the generation of noise as it is related to the diagonal coefficients of the Lighthill stress tensor. Unlike the velocity vectors, a 3D PIV system with two cameras is necessary here in order to measure the 3

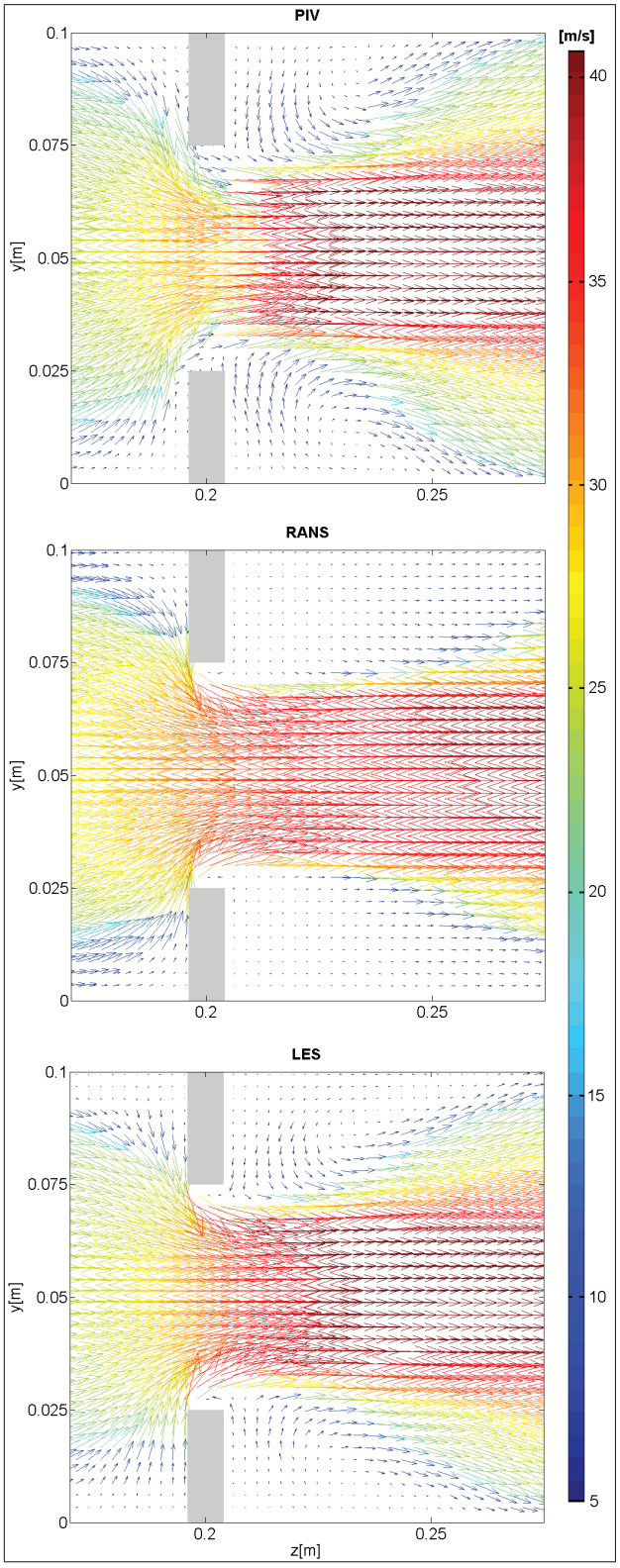

Figure 4. Velocity vectors and amplitudes.

components of the velocity. Measurements and comparisons are made over the (x_1, x_2) plane located 3 cm downstream from the diaphragm (Figure 5). Again, the LES predictions are in very good agreement with PIV results whereas RANS predictions clearly under-

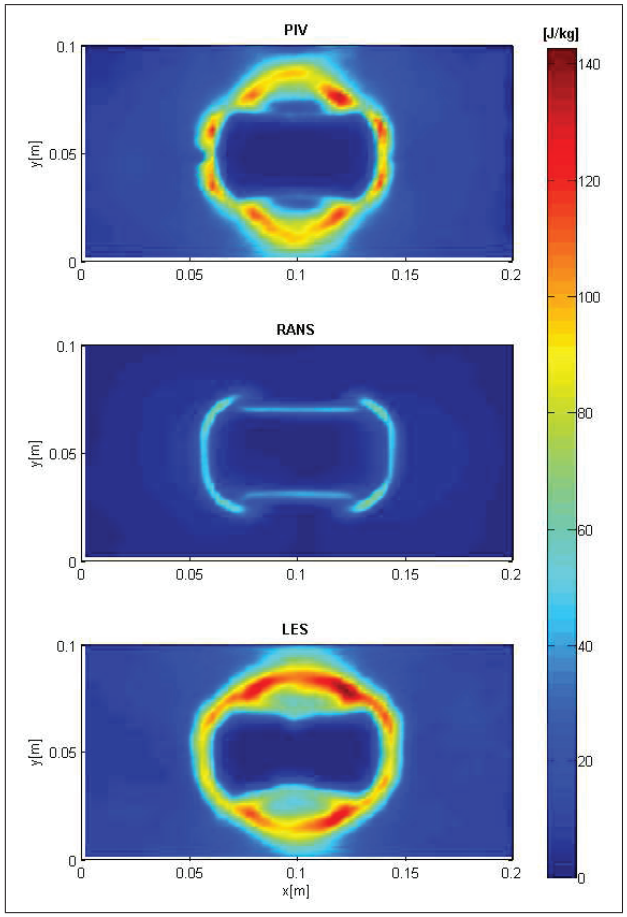

Figure 5. Mean turbulence kinetic energy.

estimate the turbulence kinetic energy.

4. Acoustic analysis

The starting point is given by the so-called Lighthill-Curle aeroacoustic analogy for the pressure fluctuations [7]. Using the tailored Green's function for the rectangular duct (we adopt the convention $\mathrm{e}^{-\mathrm{i}\omega t}$):

$$G = \sum_{mn} \frac{\Phi_{mn}(x_1, x_2)\Phi_{mn}(y_1, y_2)}{2\mathrm{i}k_{mn}} \mathrm{e}^{\mathrm{i}k_{mn}|x_3 - y_3|} \quad (3)$$

the pressure fluctuations in the duct are given by the integral representation

$$p(\boldsymbol{x}) = \int_\Gamma p \frac{\partial G}{\partial n_y} \,\mathrm{d}\Gamma_y - \int_\Omega \frac{\partial^2 T_{ij}}{\partial y_i \partial y_j} G \,\mathrm{d}\Omega_y. \quad (4)$$

Here, domain Ω extends over the volume source with $T_{ij} = \rho_0 u_i u_j$. Γ is restricted to the surface of the obstacle only as contribution from duct walls vanishes thanks to the Green's function. Formula (4) gives access to the radiated mode amplitudes (m, n) produced by the turbulent flow. However, it is an implicit integral equation as the boundary term involves the pressure flow field on the obstacle.

In the original paper [7], it is advocated that only the knowledge of the incompressible part of the pressure is sufficient for the prediction of the radiated field. This assumption which is valid for compact obstacles radiating in free space is known to break down when dealing with confined geometries [9]. To circumvent this difficulty, the pressure fluctuations on the boundary of the CFD computational domain must be solved first by solving the Curle's integral equation using the free space Green's function. The technique relies on classical BEM discretization on a coarse surface mesh obtained via interpolation of the incompressible boundary pressure (this is made via a globally conservative interpolation method from STAR-CCM+).

To summarize, the whole process consists in 4 steps: 1. interpolation to a coarse surface mesh, 2. Fourier transforms are performed for the boundary pressure, 3. a BEM approach is used to solve the pressure fluctuations to include the compressibility effects and 4. radiating modes amplitudes are computed via direct application of (4). In order to reduce the spectral fluctuations, the simulated physical time of 0.4 s (the first 0.1 s is not taken into account in our calculation) is divided into 10 segments of 0.05 s each with 1/4 overlapping. A Hanning window is applied for each segment. Thus, all computed acoustic quantities are averaged over 10 realizations.

At this stage, we shall point out that the contribution from the volume integral in (4) is usually neglected compared to the surface integral, at least under the low Mach number assumption [8], so this term is systematically discarded in our analysis.

Below the cut-off frequency of the duct (around 860 Hz), only the plane wave is allowed to propagate and (4) can be computed taking the first term of the infinite series (3). By neglecting phase differences between different regions of the diaphragm (this assumption is pratically verified for a thin obstacle), the downstream radiated pressure has the simple form:

$$p(\boldsymbol{x}) = \frac{\mathrm{e}^{\mathrm{i}kx_3}}{2A} \int_\Gamma p(\boldsymbol{y})\, n_{3y}\, \mathrm{d}\Gamma_y, \tag{5}$$

where A is the cross section area of the duct. The integral represents the drag force F_3 acting on the diaphragm. Finally, the sound power radiated by the diaphragm becomes

$$W(\omega) = \frac{\langle |F_3(\omega)|^2 \rangle}{8A\rho_0 c_0}. \tag{6}$$

Equation (6) which was first given by Morfey in 1964 [13] implies that the radiated power is identical on both sides of the obstacle. This symmetry is not necessarily preserved above cut-off.

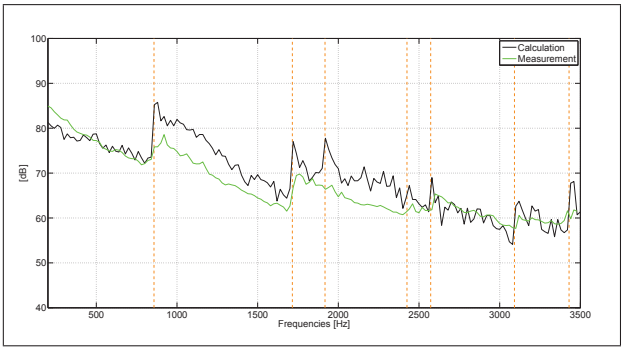

Figure 6. Computed and measured SPL at the wall 1 meter away from the diaphragm.

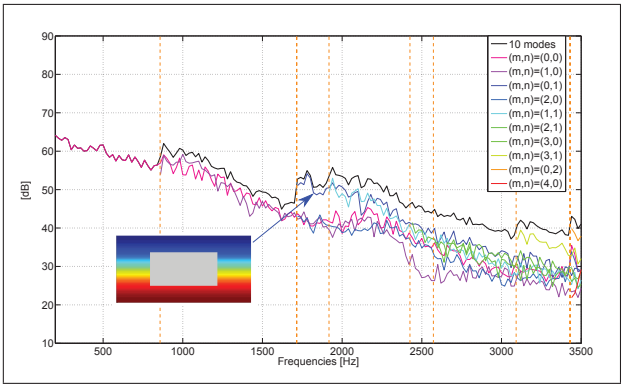

Figure 7. Modal contribution (computed).

Figure 6 shows sound pressure levels (SPL) at the wall 1 m downstream from the diaphragm (the exact location corresponds to the position of the microphone). Comparisons with measurements show fair agreement and differences do not exceed 10 dB. These differences are usually observed near cut-off frequencies (identified by orange vertical lines).

Figure 7 shows the computed modal downstream sound power. The contribution of each mode to the total sound power is rather evenly distributed except near cut-off frequencies associated with the apparition of modes (0,1) and (1,1), and in higher frequencies with modes (3,1) and (0,2). In particular, above the cut-off frequency 1715 Hz, mode (0,1) carries most of the energy. It is interesting to note that this mode matches well with the wall pressure distribution on the diaphragm with the emergence of high amplitude pressure peaks at the upper and the lower edges of the opening (in grey color).

5. Conclusion

The present work is concerned with the prediction of air flow noise in ducts. This matter is of primary concern in numerous industrial installations (pipelines, HVAC systems etc...). In many instances, the flow is characterized by a low Mach and a high

Reynolds number and the hybrid approach based on aeroacoustic analogies is well suited. The procedure consists in (i) computing the unsteady incompressible boundary pressure using a commercial software and (ii) accounting for compressibility effects by solving Curle's integral equation. The reliability of the acoustic prediction relies on the quality of aerodynamic quantities such as the turbulence kinetic energy which is known to play a significant role in the generation of noise and on an appropriate conservative interpolation technique for the boundary pressure fluctuations. Predicted Sound Pressure Levels are compared with measurements in the case of a diaphragm showing good agreements. Modal radiated sound powers are also illustrated. It is observed that an increase of sound level of nearly 10 dB can occur around cut-off frequencies of the main duct.

Work is ongoing by the present authors to investigate some interaction effects due to the presence of another obstacle inserted in the duct. In particular, the possible manifestation of self-sustained oscillations which can not be predicted by the hybrid approach should be carefully examined.

Acknowledgement

This work is part of the CEVAS (Conception d'Equipement de Ventilation d'Air Silencieux) project, funded by the Picardie Région and FEDER.

References

[1] P.A. Nelson, C.L. Morfey: Aerodynamic sound production in low speed flow ducts. Journal of Sound and Vibration **79**(2) (1981) 263–289.

[2] O. Kårekull, G. Efraimsson, M. Åbom: Prediction model of flow duct constriction noise. Applied Acoustics **82** (2014) 45–52.

[3] C.M. Mak, X. Wang, Z.T. Ai: Prediction of flow noise from in-duct spoilers using computational fluid dynamics. Applied Acoustics **76** (2014) 386–390.

[4] X. Gloerfelt, P. Lafon: Direct computation of the noise induced by a turbulent flow through a diaphragm in a duct at low Mach number. Computer and Fluids **37**(4) (2008) 388–401.

[5] M. Piellard, C. Bailly: Validation of a hybrid CAA method. Application to the case of a ducted diaphragm at low Mach number. Proceedings of the 14th AIAA/CEAS Aeroacoustics Conference, Vancouver, AIAA Paper 2008–2873, 2008.

[6] M.J. Lighthill: On sound generated aerodynamically. Part I: General theory. Proceedings of the Royal Society of London (1952) 564–587.

[7] N. Curle: The influence of solid boundaries upon aerodynamic sound. Proceedings of the Royal Society of London (1955) 505–514.

[8] G. Guilloud, C. Schram, J. Golliard: Achieving accurate and efficient prediction of HVAC diaphragm noise at realistic Reynolds and Mach numbers. Proceedings of the 15th AIAA/CEAS Aeroacoustics Conference, Miami, Florida AIAA Paper 2009–3304, 2009.

[9] C. Schram: A boundary element extension of Curle's analogy for non-compact geometries at low Mach numbers. Journal of Sound and Vibration **322** (2009) 264–281.

[10] H. Trabelsi, N. Zerbib, J.-M. Ville and F. Foucart: Méthode de mesure de la matrice de diffusion multimodale d'obstacles complexes en présence d'écoulement uniforme, CFA 2010 Congress, Lyon, 2010.

[11] S. Bennouna, B. Ouedraogo, S. Moreau, J.M Ville and O. Cheriaux: Aeroacoustic measurement of automotive HVAC in-duct elements, FAN 2015 Congress, Lyon, paper 2015-87, 2015.

[12] M. Raffel, C. Willert, J. Kompenhans: Particle Image Velocimetry: A Practical Guide, Springer-Verlag, Berlin, 1998.

[13] C.L. Morfey: Rotating pressure patterns in ducts: their generation and transmission. Journal of Sound and Vibration **1** (1964) 60–87.